Measure synchronization in a two-species bosonic Josephson junction

Jing Tian,[1,2] Haibo Qiu,[1,2,3,*] Guanfang Wang,[3] Yong Chen,[2] and Li-bin Fu[2,3,†]
[1]*College of Science, Xi'an University of Posts and Telecommunications, 710121 Xi'an, China*
[2]*Institute of Theoretical Physics, Lanzhou University, 730000 Lanzhou, China*
[3]*Institute of Applied Physics and Computational Mathematics, 100088 Beijing, China*
(Received 30 April 2013; published 6 September 2013)

Measure synchronization (MS) in a two-species bosonic Josephson junction (BJJ) is studied based on semiclassical theory. Six different scenarios for MS, including two in the Josephson oscillation regime (the zero-phase mode) and four in the self-trapping regime (the π-phase mode), are clearly shown. Systematic investigations of the common features behind these different scenarios are performed. We show that the average energies of the two species merge at the MS transition point. The scaling of the power law near the MS transition is verified and the critical exponent is $1/2$ for all of the different scenarios for MS. We also illustrate MS in a three-dimensional phase space; from this illustration, more detailed information on the dynamical process can be obtained. In particular, by analyzing the Poincaré sections with changing interspecies interactions, we find that the two-species BJJ exhibits separatrix crossing behavior at the MS transition point and such behavior depicts the general mechanism behind the different scenarios for the MS transitions. The new critical behavior found in a two-species BJJ is expected to be found in real systems of atomic Bose gases.

DOI: 10.1103/PhysRevE.88.032906 PACS number(s): 05.45.Mt, 64.60.−i, 03.75.Mn, 45.20.Jj

I. INTRODUCTION

Coupled dynamical systems can show a magnificent collective behavior called synchronization [1], a concept first shown experimentally by Huygens with two marine pendulum clocks in 1665. In recent decades, many nontrivial features have been revealed [2]. In most such studies, coupled dissipative oscillators are employed, whereas research on coupled nondissipative Hamiltonian systems is still at a primitive stage because of complications originating from Liouville's theorem [3–6]. In the latter system, a new kind of collective phenomenon called measure synchronization (MS) was found. As demonstrated by Hampton and Zanette [7], two coupled Hamiltonian systems experience a dynamical phase transition from a state in which the two Hamiltonian systems visit different phase-space domains to a state in which the two Hamiltonian systems cover an identical phase-space domain as the coupling strength increases. Such phenomena were later investigated in coupled Duffing-, φ_4-, and Frenkel-Kontorova-type Hamiltonian systems [8–10].

Experimentally, the superconducting Josephson junction is perhaps the most widely studied class in the exploration of synchronization; the superconducting Josephson junction can serve as a prime example of coupled dynamical systems. With recent experimental progress in Bose-Einstein condensates (BECs), a bosonic Josephson junction (BJJ) can be created and controlled by confining single-species BECs in a double well [11]. In a pioneering theoretical study [12], Smerzi *et al.* mapped a single-species BJJ to a classical pendulum system. Therefore, it is natural to expect that a two-species BJJ, which consists of a two-species BEC, provides a model system to study coupled dynamical systems.

The single-species BJJ is of great significance in its own right. The generalized Josephson equations describing the BJJ differ from the ones used for the superconducting Josephson junction by the presence of a nonlinear interaction term [12]. Because of this term, a single-species BJJ can exhibit a counterintuitive phenomenon called macroscopic quantum self-trapping (MQST). In a detailed analysis of this novel phenomenon [13], the Josephson oscillation (JO) regime and MQST regime can be seen in a phase-plane portrait. Additionally, through an increase in the nonlinear interaction term, the dynamical phase transition from JO to MQST will occur because of the separatrix crossing behavior in the phase space [15–18]. This dynamical phase transition behavior has been studied extensively both theoretically and experimentally [15–23].

Theoretical analysis has been extended to a two-species BJJ [24–37]. A system of equations for coupled pendula can be derived for the temporal evolution of the relative population and relative phase of each species. Many interesting tunneling effects have been found, including the symmetry restoring phase [27], mixed-Rabi-Josephson oscillation [30], and counterflow superfluidity [29]. We have studied collective modes in a two-species BJJ [38]. In addition to phase synchronization, we determined that measure synchronization can also occur. The transitions between different modes can be found by varying the interspecies interaction strength.

In this paper, we perform a systematic investigation of the measure synchronization found in such systems. Six different scenarios for MS are clearly determined. We identify that MS is a continuous phase transition, the scaling law for the MS transitions is numerically verified, and the critical exponent is $1/2$. In particular, separatrix crossing is revealed to be the dynamical mechanism behind the different scenarios for MS by Poincaré section analysis. Because experimental progress has been made in the production of two-species BECs with tunable intra- and interspecies interactions [39,40], we expect that a two-species BJJ can be realized and that the MS can thus be experimentally investigated in the near future.

This paper is organized as follows. A brief description of a two-species BJJ model is given in Sec. II. In Sec. III, different

*phyqiu@gmail.com
†lbfu@iapcm.ac.cn

scenarios of MS are introduced. Section IV presents a detailed analysis of different MS scenarios. A summary is given in Sec. V.

II. MODEL

A two-species BJJ can be experimentally realized by trapping a binary mixture of BECs in a symmetric double-well potential. By assuming that the interaction among the atoms is sufficiently weak, with the well-known two-mode approximation [12–14], the Hamiltonian in the second quantization reads

$$\hat{H} = \frac{u_a}{2N_a}[(\hat{a}_L^\dagger \hat{a}_L)^2 + (\hat{a}_R^\dagger \hat{a}_R)^2] + \frac{u_b}{2N_b}[(\hat{b}_L^\dagger \hat{b}_L)^2 + (\hat{b}_R^\dagger \hat{b}_R)^2] - \frac{v_a}{2}(\hat{a}_L^\dagger \hat{a}_R + \hat{a}_R^\dagger \hat{a}_L) - \frac{v_b}{2}(\hat{b}_L^\dagger \hat{b}_R + \hat{b}_R^\dagger \hat{b}_L) + \frac{u_{ab}}{\sqrt{N_a N_b}}(\hat{a}_L^\dagger \hat{a}_L \hat{b}_L^\dagger \hat{b}_L + \hat{a}_R^\dagger \hat{a}_R \hat{b}_R^\dagger \hat{b}_R), \quad (1)$$

where $\hat{a}_{L(R)}^\dagger$ ($\hat{a}_{L(R)}$) and $\hat{b}_{L(R)}^\dagger$($\hat{b}_{L(R)}$) are the creation (annihilation) operators for the localized modes in the left L or right R well of different species a or b, respectively. Here N_a and N_b stand for the particle numbers of species a and b. In addition, $u_\sigma = (4\pi\hbar a_\sigma N_\sigma/m_\sigma)\int |\varphi_\sigma|^4 dr$ and $u_{ab} = 2\pi\hbar a_{ab}\sqrt{N_a N_b}(\frac{1}{m_a} + \frac{1}{m_b})\int |\varphi_a|^2|\varphi_b|^2 dr$ denote the effective interaction of atomic collision between the same kind of species and between different species, respectively, with $\sigma = a,b$ indicating the species. The interactions can be either repulsive or attractive, depending on the sign of u. As demonstrated by experiments in a mixture of ^{87}Rb and ^{85}Rb [39], u_a, u_b, and u_{ab} can be tuned by the Feshbach technique. The effective Rabi frequency $v_\sigma = \int [(\hbar^2/2m_\sigma)\nabla\varphi_L \nabla\varphi_R + V(r)\varphi_L\varphi_R]dr$ describes the coupling between two wells.

Under the semiclassical limit [12–14], the dynamics of the system can be described by a classical Hamiltonian $H = \langle\Psi_{GP}|\hat{H}|\Psi_{GP}\rangle/N$, in which $|\Psi_{GP}\rangle = \frac{1}{\sqrt{N_a}}(\alpha_L \hat{a}_L^\dagger + \alpha_R \hat{a}_R^\dagger)^{N_a}|0,0\rangle \otimes \frac{1}{\sqrt{N_b}}(\beta_L \hat{b}_L^\dagger + \beta_R \hat{b}_R^\dagger)^{N_b}|0,0\rangle$ is the collective state of the N-particle system with $N = N_a + N_b$. Here $\alpha_j = |\alpha_j|e^{i\theta_{aj}}$ and $\beta_j = |\beta_j|e^{i\theta_{bj}}$ ($j = L$ or R) are four c numbers that correspond to the probability amplitudes of the two different species of atoms in the two wells. The conservation of particle numbers of each species requires $|\alpha_L|^2 + |\alpha_R|^2 = 1$ and $|\beta_L|^2 + |\beta_R|^2 = 1$.

By introducing the relative population difference $S_a = (|\alpha_L|^2 - |\alpha_R|^2)$ and $S_b = (|\beta_L|^2 - |\beta_R|^2)$ and the relative phases difference $\theta_\sigma = \theta_{\sigma L} - \theta_{\sigma R}$. We obtain the mean-field Hamiltonian [24]

$$H_{\rm tot} = H_a + H_b + H_I, \quad (2)$$

which is composed of the Hamiltonian H_σ ($\sigma = a,b$),

$$H_\sigma = -\frac{u_\sigma}{2}S_\sigma^2 + v_\sigma\sqrt{1 - S_\sigma^2}\cos\theta_\sigma, \quad (3)$$

and the coupling term

$$H_I = -u_{ab}S_a S_b. \quad (4)$$

The mean field Hamiltonian for a single-species BJJ [12,13] H_σ is well known; H_I is the coupling term. Thus a two-species BJJ is similar to two coupled single-species BJJs. It is clear that the coupling occurs because of the presence of the interspecies interaction u_{ab}.

The equations of motion can be derived by computing $\dot{\theta}_\sigma = \frac{\partial H}{\partial S_\sigma}$ and $\dot{S}_\sigma = -\frac{\partial H}{\partial \theta_\sigma}$; we obtain

$$\dot{\theta}_a = -u_a S_a - \frac{v_a S_a}{\sqrt{1 - S_a^2}}\cos\theta_a - u_{ab}S_b, \quad (5)$$

$$\dot{S}_a = v_a\sqrt{1 - S_a^2}\sin\theta_a, \quad (6)$$

$$\dot{\theta}_b = -u_b S_b - \frac{v_b S_b}{\sqrt{1 - S_b^2}}\cos\theta_b - u_{ab}S_a, \quad (7)$$

$$\dot{S}_b = v_b\sqrt{1 - S_b^2}\sin\theta_b. \quad (8)$$

The tunneling dynamics of a two-species BJJ can be described by Eqs. (5)–(8). Here the standard fourth-order Runge-Kutta method is used to obtain a numerical solution. Because we are interested in showing the effects of coupling on the dynamics of each species, the collective motion is presented by projecting the state of the full system onto the individual phase spaces, i.e., we study the trajectories $S_a(t)$ and $\theta_a(t)$ in the phase plane (S_a,θ_a) and the trajectories $S_b(t)$ and $\theta_b(t)$ in the phase plane (S_b,θ_b).

The tunneling dynamics for a single-species BJJ have been extensively studied [12–14,18–23] and studies of H_σ based on the semiclassical theory have shown that there are two distinct dynamic regimes in phase space [12,13,23]: the Josephson oscillation regime and the self-trapping regime with a strong nonlinearity ($u/v > 1$). For simplicity, the zero phase will be used to stand for the Josephson oscillation, in which θ_σ oscillates around $\theta_\sigma = 0$; the π phase stands for the self-trapping, in which θ_σ oscillates around $\theta_\sigma = \pi$. To show the coupled dynamical behavior of H_σ, we will then categorize the initial configurations of a two-species BJJ into two broad categories: (i) the zero-phase mode and (ii) the π-phase mode.

III. MEASURE SYNCHRONIZATION IN THE ZERO- AND π-PHASE MODES

A. The zero-phase mode

First, we present measure synchronization in the zero-phase mode, that is, the mode in which θ_σ oscillates around $\theta_\sigma = 0$. The initial conditions $(S_a,\theta_a,S_b,\theta_b)$ are (0.2,0.0,0.4,0.0), $u_a = u_b = 1.2$, and $v_a = v_b = 1$.

1. With repulsive interactions ($u_{ab} > 0$)

Figures 1(a)–1(c) show the evolution process for MS with repulsive interspecies interactions ($u_{ab} > 0$). By increasing the coupling strength u_{ab}, we draw orbits on the (S_σ,θ_σ) ($\sigma = a,b$) phase plane of the two subsystems. For $u_{ab} = 0$, as shown in Fig. 1(a), these initial conditions correspond to two different quasiperiodic orbits, which cover closed curves in green and black. For $u_{ab} > 0$, the two closed curves are replaced with two smooth quasiperiodic trajectories wandering in two distinctive phase-space domains, which are ring shaped. As u_{ab} increases, the two phase-space domains first evolve such that the external border of the inner domain approaches the internal border of the outer domain and the two approach each other until $u_{ab} = 0.0086$, at which point the two approaching boundaries

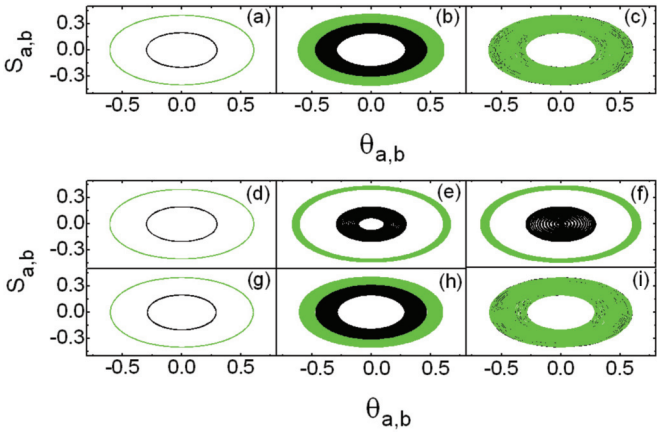

FIG. 1. (Color online) Phase-space domains of the two species in the zero-phase mode. The two species are represented by green and black. The initial configuration $(S_a,S_b,\theta_a,\theta_b)$ is set to be (0.2,0.4,0,0). MS for repulsive u_{ab}: (a) $u_{ab}=0$, (b) $u_{ab}=0.0086$, and (c) $u_{ab}=0.009$. MS for attractive u_{ab}: (d) $u_{ab}=0$, (e) $u_{ab}=-0.01$, (f) $u_{ab}=-0.0325$, (g) $u_{ab}=-0.0625$, (h) $u_{ab}=-0.0738$, and (i) $u_{ab}=-0.08$.

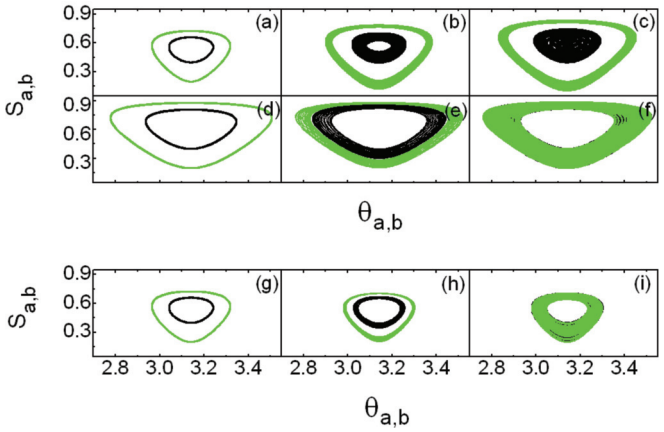

FIG. 2. (Color online) Phase-space domains of the two species in the localized π-phase mode. The two species are represented by green and black. The initial configuration $(S_a,S_b,\theta_a,\theta_b)$ is set to be $(0.2,0.4,\pi,\pi)$. MS for repulsive u_{ab}, (a) $u_{ab}=0$, (b) $u_{ab}=0.03$, (c) $u_{ab}=0.0737$, (d) $u_{ab}=0.1498$, (e) $u_{ab}=0.1621$, and (f) $u_{ab}=0.1622$, and attractive u_{ab}, (g) $u_{ab}=0$, (h) $u_{ab}=-0.01$, and (i) $u_{ab}=-0.0123$.

are almost in contact [Fig. 1(b)]. Then a sudden change occurs as u_{ab} increases further, as shown in Fig. 1(c). The two formally well-separated phase-space domains merge and cover the phase-space domains with identical invariant measure [7]. This dynamical phase transition of the two phase-space domains marks the transition to measure synchronization. The evolution process described above is identical to that described previously [7–9], which we will call typical MS hereafter.

2. *With attractive interactions ($u_{ab}<0$)*

Figures 1(d)–1(i) show the evolution process with increasing strength of attractive interspecies interactions. As a starting point, in Fig. 1(d) we plot the orbits for each species at zero coupling. For $u_{ab}<0$, as u_{ab} decreases, we see that this evolution process is quite different from the typical MS. The two phase-space domains first evolve in the opposite direction; the internal border of the inner ring approaches the center of the phase-space domain, whereas the external border of the outer ring expands [Fig. 1(e)]. For $u_{ab}=-0.0325$, the internal border of the inner ring finally reaches the center of the phase space [Fig. 1(f)]. Then, as u_{ab} decreases, these two rings gradually thin until $u_{ab}=-0.0625$; at this point, the two rings again become two curves [Fig. 1(g)], which appear to be similar to $u_{ab}=0$ [Fig. 1(d)]. Additionally, as u_{ab} continues to decrease [Figs. 1(g)–1(i)], the evolution process becomes identical to that for the typical MS process [as described in Figs. 1(a)–1(c)].

B. Localized π-phase mode

Here we present measure synchronization in the π-phase mode, in which θ_σ oscillates around $\theta_\sigma=\pi$. The initial conditions $(S_a,\theta_a,S_b,\theta_b)$ are $(0.2,\pi,0.4,\pi)$, $u_a=u_b=1.2$, and $v_a=v_b=1$.

1. *With repulsive interaction ($u_{ab}>0$)*

Figures 2(a)–2(f) show the evolution process for MS with repulsive interspecies interactions ($u_{ab}>0$). For $u_{ab}=0$, as shown in Fig. 2(a), these initial conditions correspond to two different quasiperiodic orbits, which cover closed curves in green and black, and the two curves have an inverted-triangle shape. By increasing the coupling strength, we can see that the two inverted triangles broaden in such a way that the two embedded phase-space domains evolve in opposite directions [Fig. 2(b)] and the internal border of the original inner inverted triangle approaches the center of the phase space. At $u_{ab}=0.0737$, the inner phase-space domain reaches the center [Fig. 2(c)]. Subsequently, the two phase-space domains approach one another until they make contact before the MS transition at $u_{ab}=0.1621$; in this evolution process, there is also be a moment at which the phase-space domains become closed curves again [Fig. 2(d)]. This scenario is similar to the scenario for attractive interactions in the zero-phase mode. The most obvious difference is that the phase-space domains no longer have conserved boundaries: As the coupling strength increases, the area expands.

2. *With attractive interaction ($u_{ab}<0$)*

Figures 2(g)–2(i) show the scenario with increasing strength of attractive interspecies interactions. This scenario is very similar to the scenario for typical MS. We find that as the coupling strength increases, the two phase-space domains approach each other until MS occurs at $u_c=-0.0123$.

C. Nonlocalized π-phase mode

In the π-phase mode, a new type of coherent evolution process is found, as shown in Fig. 3, for the initial conditions $(S_a,\theta_a,S_b,\theta_b)$ of $(0.2,\pi,-0.4,\pi)$. At $u_{ab}=0$, compared with the localized π-phase mode, these initial conditions also correspond to two closed curves, but with one curve on top of the other [Fig. 3(a)].

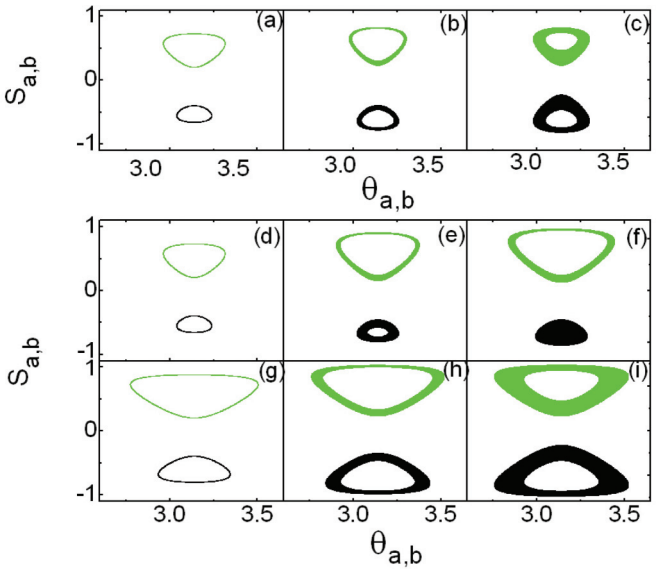

FIG. 3. (Color online) Phase-space domains of the two species in the nonlocalized π-phase mode. The two species are represented by green and black. The initial conditions $(S_a,\theta_a,S_b,\theta_b)$ are taken to be $(0.2,\pi,-0.4,\pi)$ in the π-phase mode. Nonlocal MS for repulsive u_{ab}, (a) $u_{ab}=0$, (b) $u_{ab}=0.01$, and (c) $u_{ab}=0.0123$, and attractive u_{ab}, (d) $u_{ab}=0$, (e) $u_{ab}=-0.03$, (f) $u_{ab}=-0.0737$, (g) $u_{ab}=-0.1498$, (h) $u_{ab}=-0.1621$, and (i) $u_{ab}=-0.1622$.

As the strength of repulsive interspecies interactions increase, the phase-space domains of the two species become more comparable in area until u_{ab} reaches a critical value ($u_{ab}=0.0123$) [Fig. 3(b)]; then, a sudden change occurs, as shown in Fig. 3(c), and the two phase-space domains have the same area. However, in contrast to Fig. 2(i), the phase-space domain of each species lies symmetrically on both sides of the line $S=0$ [Fig. 3(c)].

As the strength of attractive interspecies interactions increases, we find another scenario for the transition behavior that ends in a similar state [Fig. 3(i)]. Interestingly, we note that this scenario has many features in common with the scenario shown in Figs. 2(a)–2(g). One major difference is the structure of the phase-space domains: One structure goes from top to bottom, whereas the other structure is embedded.

Comparing Figs. 2 and 3, we can see that each phase diagram corresponds to u_{ab} values with the same magnitude but with opposite sign. This result can be understood by analyzing Eqs. (2)–(4). If we set s_a and s_b to have opposite signs and let u_{ab} also have a value with opposite sign, the coupling term H_I does not change and neither H_a or H_b changes. The two different initial conditions with opposite signs for the interspecies interactions correspond to the same Hamiltonian and consequently have the same dynamic evolution.

IV. ANALYSIS

Below we will explore the nature of the MS found for a two-species BJJ in detail.

A. Energy characteristics

For the two groups of MS scenarios that have been found, the zero- and π-phase modes, we analyze the energy function for each species $E_{a,b}$ and observe how the energy function changes with interspecies interactions. Here

$$E_{a,b}=-\frac{u_{a,b}}{2}S_{a,b}^2+v_{a,b}\sqrt{1-S_{a,b}^2}\cos\theta_{a,b}. \qquad (9)$$

In Fig. 4 we plot the energy function for each species with different interspecies interaction strengths below u_c for the initial configuration in the zero-phase mode and

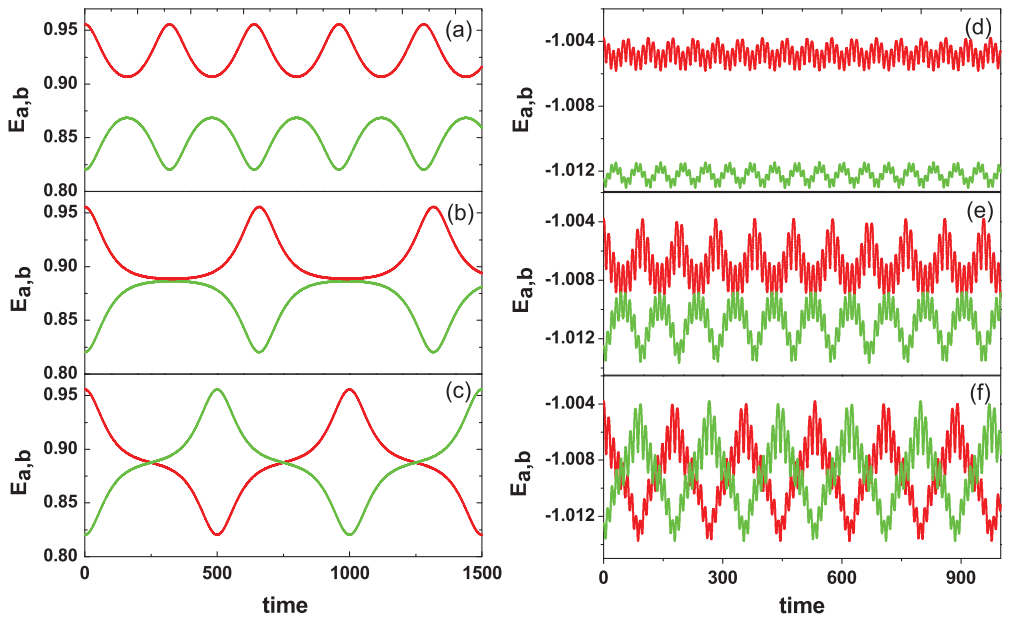

FIG. 4. (Color online) Evolution of energy functions for the two species for (a)–(c) the zero-phase mode and (d)–(f) the π-phase mode. Before MS is achieved ($u_{ab}<u_c$), the two species have different energy variations; after MS is achieved ($u_{ab}\geqslant u_c$), the two energy variations would be the same. The demixing to mixing feature of MS transitions can be clearly seen.

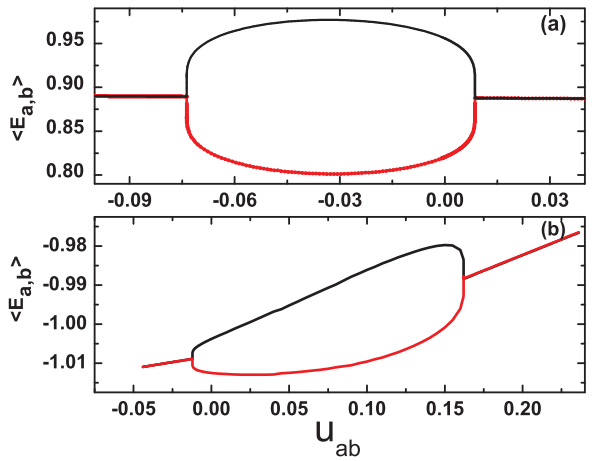

FIG. 5. (Color online) Average energies of the two species in the zero- and π-phase modes. The two subsystems would have equal averaged energy once MS is achieved in (a) the zero-phase mode and (b) the π-phase mode.

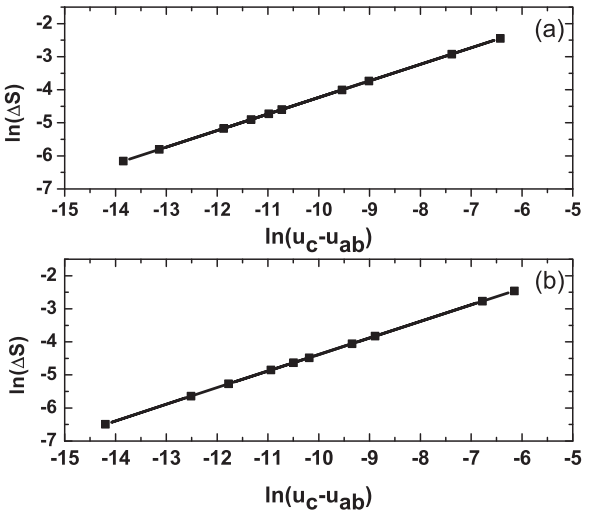

FIG. 6. Scaling relation of $\triangle S \propto (u_{ab} - u_c)^{1/2}$ for (a) the zero-phase mode with repulsive interaction and (b) the π-phase mode with repulsive interaction.

π-phase mode for repulsive interspecies interaction. Before measure synchronization, E_a and E_b do not overlap at all. As u_{ab} continues to increase, the difference between the lower boundary of the initially higher-energy species and the upper boundary of the initially lower-energy species becomes smaller and smaller. When u_{ab} reaches the transition point u_c, $E_{a,b}$ suddenly has the same range of energy variation. This evolution process is shown in Figs. 4(a)–4(c) for the zero-phase mode and in Figs. 4(e)–4(g) for the π-phase mode. The demixing to mixing feature of the MS transitions can be clearly seen in these figures.

To describe MS in the context of our physical model, the average energy of a single-species BJJ is defined to be

$$\langle E_{a,b} \rangle = \frac{1}{T} \int_0^T E_{a,b} dt. \tag{10}$$

In Fig. 5(a) we show the average energy $\langle E_a \rangle$ and $\langle E_b \rangle$ as a function of interspecies interactions u_{ab} in the zero-phase mode. It is clear that there are sharp transitions at $u_{ab} = u_c = 0.0086$ and $u_{ab} = u_c = -0.0738$ for the repulsive and attractive interactions, respectively. Below u_c ($|u_{ab}| < |u_c|$), there is a finite difference between E_a and E_b, whereas above u_c ($|u_{ab}| > |u_c|$), both species have identical average energies. Figure 5(b) shows the plot for the π-phase mode. The correspondence of the MS transition with the sudden merging of the average energies is also clearly shown. In addition, we find that the average energies change in the π-phase mode, even in the measure-synchronized state, whereas in the zero-phase mode, the average energies remain fixed.

B. Critical behavior

The critical behavior of MS has been studied previously. In the seminal work in [7], Hampton and Zanette introduced an order parameter to study the critical logarithmic singularity; however, they did not find the scaling law and the critical exponent because of the order parameter, which is an averaged quantity, that was chosen for the calculation. In Ref. [8], through the computation of the interaction energy and the phase dynamics of the oscillators, the scaling law behind MS in coupled φ_4 systems was extensively discussed and different scaling laws were numerically verified before and after MS. The critical exponents are $1/3$ and $1/2$.

Here we studied the critical behavior of MS in a two-species BJJ. We confirmed that there are scaling laws in this system. As the two phase-space domains approach each other, we noticed that the two phase-domain boundaries are getting close to contact and there is a scaling relation behind this process. By computing the distance between $\triangle S$ and the two approaching boundaries on the $S_{a,b}$ axes, we find the scaling relation between $\triangle S$ and $u_{ab} - u_c$; this relation is $\triangle S \propto (u_{ab} - u_c)^{1/2}$ and the critical exponent is $1/2$. Figure 6(a) shows the scaling relation for the zero-phase mode with repulsive interactions and Fig. 6(b) shows the scaling relation for the π-phase mode with repulsive interactions. For the other scenarios, we have verified that the critical exponents are all identical and are $1/2$.

C. Three-dimensional description

Previous work on MS only studied the two-dimensional projected phase-space domains of the coupled-Hamiltonian system. However, this projection could not be a complete description of the dynamical behavior because the dynamics of the two-coupled Hamiltonian actually take place in a four-dimensional phase space $(S_a, \theta_a, S_b, \theta_b)$. In the absence of dissipation, energy constrains the motion of the system to a three-dimensional energy hypersurface of the four-dimensional phase space. To gain the most insight into MS, we can use a three-dimensional description of MS.

By taking the initial configuration in the zero-phase mode as an example, we provide a three-dimensional description of measure synchronization in Fig. 7. First, we choose two different sets of coordinate axes: $(S_\sigma, \theta_\sigma, S_{\bar{\sigma}})$ and $(S_{\bar{\sigma}}, \theta_{\bar{\sigma}}, S_\sigma)$ with $\sigma = a, b$. The corresponding initial conditions and the coupling u_{ab} are identical to those in Fig. 1.

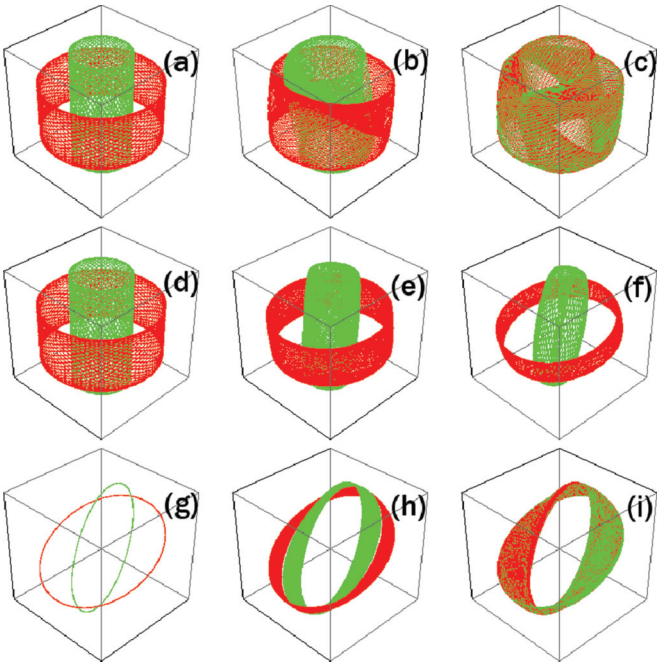

FIG. 7. (Color online) Three-dimensional view of MS for a two-species BJJ in the zero-phase mode. Two different colors represent two different choices of the three-dimensional axes: The green one is drawn on axes (S_a,θ_a,θ_b) and the red one is drawn on axes (S_b,θ_b,θ_a). (c) and (i) show measure synchronized states.

With repulsive interspecies interactions ($u_{ab} > 0$), the evolution process of the three-dimensional phase space is shown in Figs. 7(a)–7(c); these figures show side views of the two manifolds in the three-dimensional phase-space representation and top views corresponding to the figures shown in Figs. 1(a)–1(c). In Fig. 7(a), for $u_{ab} = 0$, there are two well-separated manifolds, with one manifold around the other. For $u_{ab} = 0.0086$, as shown in Fig. 7(b), the two manifolds are close to each other but are still separated from one another. However, with $u_{ab} > 0.0086$, as shown in Fig. 7(c) ($u_{ab} = 0.009$), we see that the two manifolds completely overlap; this overlap indicates the measure-synchronized states in the three-dimensional phase-space representation.

With attractive interspecies interactions ($u_{ab} < 0$), the evolution process of the three-dimensional phase space is shown in Figs. 7(d)–7(i). The process shown in Figs. 7(d)–7(i) is not as direct as in case of the repulsive interspecies interactions because initially the inner phase-space volume shrinks in size [Figs. 7(d)–7(g)]; then this volume expands continuously until it achieves the measure-synchronized states [Fig. 1(i)]. There we can see some behaviors that are not apparent on the two-dimensional map; for example, although Figs. 1(g) and 1(d) appear to be exactly identical, they are actually very different, as shown in the three-dimensional representation: Fig. 7(d) shows quasiperiodic states, whereas Fig. 7(g) shows periodic states. The volume of the synchronized state also apparently changed; however, in the two-dimensional projection, we cannot see many of these changes.

To summarize, a three-dimensional view of MS is given. It is observed that as MS is attained, the two energy manifolds in the phase space $(S_\sigma,\theta_\sigma,S_{\bar{\sigma}})$ completely overlap. This result provides a more intuitive picture of MS compare with the two-dimensional projection and some features that we do not see in the two-dimensional phase space are presented. These features include the difference between the quasiperiodic state and periodic state [Figs. 1(d) and 1(g)] and the changing volume of the manifolds as u_{ab} increases can be seen clearly. These results help us understand the measure invariance of the two-dimensional phase-space domains after MS is achieved because the phase-space domains can be seen to be the projection of the two energy manifolds on a two-dimensional phase plane.

D. Poincaré section analysis

Measure synchronization is a dynamical phase transition phenomenon in coupled Hamiltonian systems, so naturally, we ask how this phenomenon occurs. We find that the answer can be revealed through the analysis of the Poincaré maps of the system.

The procedure for our analysis can be demonstrated for the example of the repulsive interactions in the zero-phase mode [Fig. 8(a)]. First, we solve the canonical equations (5)–(8); then we take the section slice of (S_a,θ_a) at each time for which $\theta_b = 0.0$ and $\dot{\theta}_b > 0$; the section slice taken in this procedure is marked with black dots. Simultaneously, we also take the section slice of (S_b,θ_b) at each time for which $\theta_a = 0.0$ and $\dot{\theta}_a > 0$; this type of section slice is marked with green dots. In Fig. 8(a), different curves with the same color are drawn for different values of u_{ab} that we chose. For the black dotted curves, with $u_{ab} = 0.001$, the corresponding Poincaré section is the innermost, closed, ring-shaped curve. As the coupling intensity increases, this ring-shaped curve expands until u_{ab} reaches u_c ($u_c = 0.008\,621$); at u_c, the section slice corresponds to the separatrix, which is marked with red dots. For $u_{ab} > u_c$, the section slice is shaped like a crescent moon and shrinks in size as u_{ab} increases further. The green dotted curves are drawn for the same chosen set of u_{ab} values; the outermost curve corresponds to the Poincaré section for $u_{ab} = 0.001$. Conversely, we observe that this ring-shaped Poincaré section shrinks in size before u_{ab} reaches u_c and at u_c, the separatrix is also shown; beyond u_c, the ring-shaped curve also assumes a crescent moon shape and shrinks in size as u_{ab} increases further. We note that the separatrix marks the transition from the localized to the shared phase space. After the measure synchronization of the two coupled Hamiltonian systems for $u_{ab} > u_c$, the green dotted and black dotted trajectories with the same coupling intensities merge completely.

Similarly, we perform Poincaré section analysis for the other scenarios. Figure 8(b) shows the result for the zero-phase mode with attractive interspecies interactions and Figs. 8(c) and 8(d) show the results of Poincaré section analysis for the π-phase mode with attractive interspecies interactions and repulsive interspecies interactions, respectively. We can see that in all cases separatrices mark the onset of measure synchronization.

In summary, through Poincaré section analysis, we have shown that a two-species BJJ exhibits separatrix crossing behavior at the critical interspecies interaction of the MS transition. Therefore, we identified the separatrix crossing to be the underlying dynamical mechanism of MS.

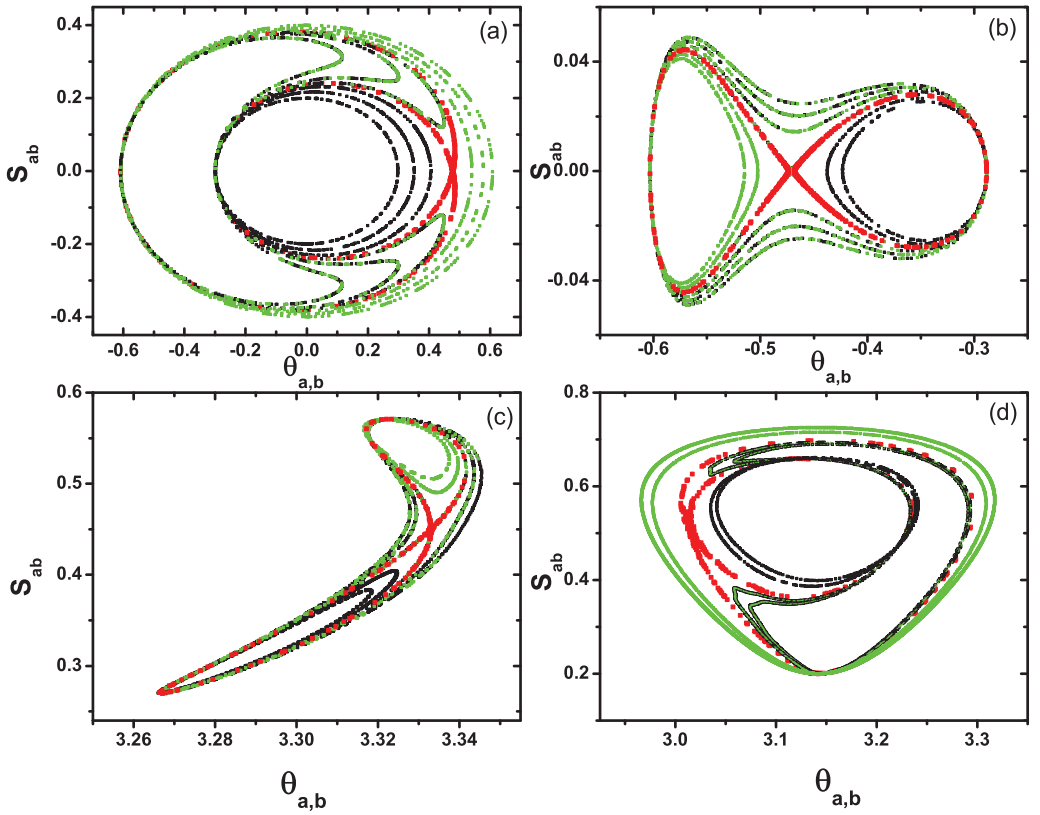

FIG. 8. (Color online) Poincaré section analysis for different scenarios of MS shown in Figs. 1 and 2. The red curves with X-point geometry mark the MS transitions, which correspond to separatrices.

V. CONCLUSION

Measure synchronization in a two-species BJJ has been systematically studied. Six different scenarios of MS, including two in the zero-phase mode and four in the localized and nonlocalized π-phase modes, have been characterized and some common features behind have been revealed. We have found that the MS transition corresponds to the sudden merger of average energies of the two species. The power law scaling behind the MS transition has been verified, which is the same for the different scenarios, and the critical exponent is $1/2$. Furthermore, we have given a three-dimensional view of MS that provides a more intuitive picture of MS. Some features that we will not see in the two-dimensional phase space are revealed. In particular, by using the Poincaré section analysis, it has been clearly shown that a two-species BJJ exhibits separatrix crossing behavior at u_c. We conclude that separatrix crossing is the general mechanism behind the different scenarios of MS transitions found in the two-species BJJ.

ACKNOWLEDGMENTS

We thank Qiang Gu for a critical reading of the manuscript. This work was supported by the National Natural Science Foundation of China (Grants No. 11104217 and No. 11205121), the Science Plan Foundation Office of the Education Department of Shaanxi Province (Grant No. 11JK0555), and the Youth Foundation of XUPT under Grants No. 0001295 and No. 0001287.

[1] Y. Kuramoto, *Chemical Oscillations, Waves and Turbulence* (Springer, Berlin, 1984); A. Pikovsky, H. Rosenblum, and J. Kurths, *Synchronization: A Universal Concept in Nonlinear Sciences* (Cambridge University Press, Cambridge, 2001).

[2] V. Hakim and W. J. Rappel, Phys. Rev. A **46**, R7347 (1992); K. Okuda, Physica D (Amsterdam) **63**, 424 (1993); N. Nakagawa and Y. Kuramoto, Prog. Theor. Phys. **89**, 313 (1993); Physica D (Amsterdam) **75**, 74 (1994); S. K. Han, C. Kurrer, and Y. Kuramoto, Phys. Rev. Lett. **75**, 3190 (1995).

[3] H. Morita and K. Kaneko, Phys. Rev. Lett. **96**, 050602 (2006).

[4] D. H. Zanette and A. S. Mikhailov, Phys. Lett. A **235**, 135 (1997).

[5] K. K. Likharev, *Dynamics of Josephson Junctions and Circuits* (Gordon and Breach, New York, 1986).

[6] B. Pannetier, A. Bezryadin, and E. Eichenberger, in *ICTP Workshop on Josephson Junction Arrays, Trieste, 1995*, edited by H. A. Cerdeira and S. R. Shenoy, special issue of Physica B **222**, 253 (1996).

[7] A. Hampton and D. H. Zanette, Phys. Rev. Lett. **83**, 2179 (1999).

[8] X. Wang, M. Zhan, C.-H. Lai, and H. Gang, Phys. Rev. E **67**, 066215 (2003).

[9] U. E. Vincent, New J. Phys. **7**, 209 (2005).
[10] J. R. Zhang, H. Jiang, Y. Yang, W. S. Duan, and J. M. Chen, Phys. Scr. **86**, 065602 (2012).
[11] M. Albiez, R. Gati, J. Folling, S. Hunsmann, M. Cristiani, and M. K. Oberthaler, Phys. Rev. Lett. **95**, 010402 (2005).
[12] A. Smerzi, S. Fantoni, S. Giovanazzi, and S. R. Shenoy, Phys. Rev. Lett. **79**, 4950 (1997).
[13] S. Raghavan, A. Smerzi, S. Fantoni, and S. R. Shenoy, Phys. Rev. A **59**, 620 (1999).
[14] A. J. Leggett, Rev. Mod. Phys. **73**, 307 (2001).
[15] T. Zibold, E. Nicklas, C. Gross, and M. K. Oberthaler, Phys. Rev. Lett. **105**, 204101 (2010).
[16] H. Hennig, D. Witthaut, and D. K. Campbell, Phys. Rev. A **86**, 051604(R) (2012).
[17] G. J. Krahn and D. H. J. O'Dell, J. Phys. B **42**, 205501 (2009).
[18] M. Chuchem, K. Smith-Mannschott, M. Hiller, T. Kottos, A. Vardi, and D. Cohen, Phys. Rev. A **82**, 053617 (2010).
[19] K. Sakmann, A. I. Streltsov, O. E. Alon, and L. S. Cederbaum, Phys. Rev. Lett. **103**, 220601 (2009).
[20] R. Hipolito and A. Polkovnikov, Phys. Rev. A **81**, 013621 (2010).
[21] B. Juliá-Díaz, D. Dagnino, M. Lewenstein, J. Martorell, and A. Polls, Phys. Rev. A **81**, 023615 (2010).
[22] S. Levy, E. Lahoud, I. Shomroni, and J. Steinhauer, Nature (London) **449**, 579 (2007); Y. Shin, G. B. Jo, M. Saba, T. A. Pasquini, W. Ketterle, and D. E. Pritchard, Phys. Rev. Lett. **95**, 170402 (2005); L. J. LeBlanc, A. B. Bardon, J. McKeever, M. H. T. Extavour, D. Jervis, J. H. Thywissen, F. Piazza, and A. Smerzi, *ibid.* **106**, 025302 (2011).
[23] L. Fu and J. Liu, Phys. Rev. A **74**, 063614 (2006).
[24] S. Ashhab and C. Lobo, Phys. Rev. A **66**, 013609 (2002).
[25] X. Q. Xu, L. H. Lu, and Y. Q. Li, Phys. Rev. A **78**, 043609 (2008).
[26] H. T. Ng and P. T. Leung, Phys. Rev. A **71**, 013601 (2005).
[27] I. I. Satija, R. Balakrishnan, P. Naudus, J. Heward, M. Edwards, and C. W. Clark, Phys. Rev. A **79**, 033616 (2009).
[28] G. Mazzarella, M. Moratti, L. Salasnich, M. Salerno, and F. Toigo, J. Phys. B **42**, 125301 (2009).
[29] G. Mazzarella, M. Moratti, L. Salasnich, and F. Toigo, J. Phys. B **43**, 065303 (2010).
[30] G. Mazzarella, B. Malomed, L. Salasnich, M. Salerno, and F. Toigo, J. Phys. B **44**, 035301 (2011).
[31] B. Juliá-Díaz, M. Guilleumas, M. Lewenstein, A. Polls, and A. Sanpera, Phys. Rev. A **80**, 023616 (2009).
[32] B. Sun and M. S. Pindzola, Phys. Rev. A **80**, 033616 (2009).
[33] A. Naddeo and R. Citro, J. Phys. B **43**, 135302 (2010).
[34] M. C. Tichy, J. F. Sherson, and K. Mølmer, Phys. Rev. A **86**, 063630 (2012).
[35] S. N. Burmistrov, Phys. Rev. A **83**, 063627 (2011).
[36] B. Chatterjee, I. Brouzos, L. S. Cao, and P. Schmelcher, Phys. Rev. A **85**, 013611 (2012).
[37] L. H. Lu, X. Q. Xu, and Y. Q. Li, J. Phys. B **44**, 145301 (2011).
[38] H. Qiu, J. Tian, and L.-B. Fu, Phys. Rev. A **81**, 043613 (2010).
[39] S. B. Papp and C. E. Wieman, Phys. Rev. Lett. **97**, 180404 (2006); S. B. Papp, J. M. Pino, and C. E. Wieman, *ibid.* **101**, 040402 (2008); G. Thalhammer, G. Barontini, L. De Sarlo, J. Catani, F. Minardi, and M. Inguscio, *ibid.* **100**, 210402 (2008); D. J. McCarron, H. W. Cho, D. L. Jenkin, M. P. Köppinger, and S. L. Cornish, Phys. Rev. A **84**, 011603(R) (2011).
[40] C. Chin, R. Grimm, P. Julienne, and E. Tiesinga, Rev. Mod. Phys. **82**, 1225 (2010).